INCREASING THE PINNING FORCE AND CRITICAL CURRENTS IN YBaCuO-TYPE SUPERCONDUCTORS*

Krzysztof Rogacki

Institute of Low Temperature and Structure Research
Polish Academy of Sciences, Wrocław, Poland

Bogdan Dabrowski

Institute of Physics, Polish Academy of Sciences, Warsaw, Poland

Received 2 April 2026, accepted 21 April 2026, published online 15 May 2026

In this work, we conducted a detailed analysis of the types of mechanisms by which vortex lines interact with pinning centers generated in $YBa_2Cu_3O_{7-d}$ (Y123) single crystals by annealing in high oxygen pressure and Mo-substitution. Our analysis is based on the properties of these centers influencing the pinning force. Based on the previously obtained results on the dependence of the critical current density, j_c, on the magnetic field, $j_c(H)$, we determined j_c as a function of temperature, $j_c(T)$, for different H, which we used to answer the question of which pinning mechanism, δl or δT_c, dominates in Y123 single crystals. Our results differ both quantitatively and qualitatively from those previously reported, which we explain by understanding the types of pinning centers generated in studied materials. Our results provide a better understanding of the phenomena leading to significant increases in critical currents in Y123 and thus allow for better prediction of pinning centers that operate effectively under desired magnetic fields and temperatures.

DOI:10.5506/APhysPolB.57.5-A7

1. Introduction

Copper–oxide superconductors constitute an extremely important family of high-temperature superconductors (HTSCs), represented by many materials, including compounds of the $YBa_2Cu_3O_{7-d}$ (Y123) type, which continue to surprise with increasingly significant applications [1–4]. The reasons that prevent the widespread use of these compounds on a large scale are their ceramic nature and layered structure and, therefore, considerable anisotropy of superconducting properties. These compounds have a perovskite structure with a characteristic cell consisting of conducting layers composed of

* Presented at the Concepts in Strongly Correlated Quantum Matter Conference (CSCQM), Kraków, Poland, 20–22 November, 2025.

Y ion placed between two CuO_2 planes (Y–Cu–O conducting blocks) and quasi-insulating Ba–Cu–O regions containing CuO chains [5]. Since the coherence length for superconductivity, ξ, is comparable to or smaller than the distance between the Y–Cu–O blocks (metallic and superconducting) at temperatures far from the critical temperature, T_c, these materials have quasi-2-dimensional (2D) properties due to superconductivity [6, 7].

There are three structural forms of these compounds that differ in the ratio of yttrium, barium, and copper, Y123, $YBa_2Cu_4O_8$ (Y124), and $Y_2Ba_4Cu_7O_y$ (Y247), but certainly the most promising compound for applications is still the $YBa_2Cu_3O_{7-d}$, whose potential for use in high-energy electrical transport has been indicated for a long time [8]. Its critical temperature is slightly above 90 K with optimal oxygen doping, and in addition, it has an extremely high irreversibility field, H_{irr}, and the critical current density, j_c, which at liquid nitrogen temperature are approximately 20 T and 10^5 A/cm^2, respectively [9]. After the initial commercialization of HTSCs, the challenge arose of how to increase their critical parameters, including the critical current density. In the case of Y123, the only superconductor that can be widely used in high-magnetic fields at liquid nitrogen temperature, this is particularly important due to the high cost of producing useful superconducting tapes that require complex texturing and, further increasing the cost, inclusion of the rare-earth ions, like Gd in place of Y [10]. Ultimately, increasing the critical current density will make Y123 a more competitive material in the market, also by reducing the cost of devices that transmit energy and generate high-magnetic fields, including significantly reducing the size of tokamaks for thermonuclear fusion [11] and small magnets for various innovative applications [12].

The effectiveness of pinning centers induced by Mo substitution in raising the j_c in Y123-type materials has been demonstrated in several studies conducted on powder samples [13–15]. As these studies show, Mo substitutes partially in the CuO chains in place of CuO_4 in form of MoO_6 octahedra, which could be effective pinning centers at lower temperatures, where the coherence length is comparable to the size of the octahedra. It turned out that under appropriate synthesis conditions, two MoO_6 octahedra form a Mo_2O_{11} dimer (see Fig. 1 in [16]), which induces a crystal lattice defect with a size of several unit cells corresponding to the coherence length at elevated temperatures, close to the boiling point of nitrogen, and is therefore a good pinning center at these temperatures [14, 15].

We conducted further studies on the role of Mo introduced into Y123 on single crystals, which allowed us to better understand the vortex pinning mechanism by eliminating the influence of grain boundaries on the observed properties [16, 17]. This also allowed for a better definition of the type of pinning centers present there through the broader use of scaling procedures

and enabled the determination of critical current anisotropy. Furthermore, we were able to characterize the temperature-magnetic field regions dominated by the specific types of pinning centers, which is important because it allows for the design of materials with the desired parameters for use at specific temperatures and magnetic fields.

In the present work, we extend our research to analyze previously obtained experimental results to determine one of the two main types of pinning occurring in superconductors, referred to as δl and δT_c: the pinning resulting from fluctuations in the electron mean free path and the pinning induced by fluctuations in the superconducting transition temperature [18]. As can be seen from the analysis of the $j_c(H)$ dependencies for our single crystals, the presence of a strong peak effect (the fishtail effect or second magnetization peak on the $M(H)$ dependencies) would suggest the validity of δT_c pinning [19]. To our surprise, the nature of the $j_c(t)/j_c(0)$ dependencies, where $t = T/T_c$, is clearly different and corresponds to δl pinning, although it does not allow for full scaling.

2. Experimental

Single crystals of the composition $YBa_2Cu_{3-x}Mo_x O_{7-d}$ with a nominal Mo content in the range $0 \leq x \leq 0.12$ were synthesized by the self-flux growth method [16]. Normal pressure annealing was performed in pure oxygen for 12 h at 300–500°C, followed by slow cooling to room temperature. Low- and high-pressure annealing was performed in a home-made apparatus in pure oxygen at 130–140 bar (LPA) at 250–400°C and 260–270 bar (HPA) at 500°C, followed by slow cooling to room temperature. Detailed descriptions of the crystal preparation and characterization procedures are provided in Refs. [16, 17] and references therein. For our studies, four single crystals were selected: two without Mo (Y123–LPA, Y123–HPA) and two with Mo added (YMo2–LPA, YMo2–LPA–HPA), where the Mo content was $x = 0.03$ (1 at.%), which corresponds to a 3 at.% substitution of Mo in the CuO chains and to about 1/133 of the planar density of the Mo_2O_{11} dimmers. "Pure" single crystals (without Mo) had dimensions on average of $1 \times 1 \times 0.1$ mm^3, and those with substituted Mo were slightly larger.

Magnetization hysteresis loops $M(H)$ were measured for a set of 3–4 single crystals from each batch, and the results appear to be batch typical. These loops were obtained in the temperature range 2–90 K and in magnetic fields up to 7 and 14 T, using Quantum Design MPMS and PPMS magnetometers, respectively. The full results and their analysis are presented in [17]. The obtained magnetization loops were used to calculate the critical current density based on the Bean critical state model [20]. A detailed discussion of the procedure used, and details related to the consideration of a single crystal shape in the calculations of j_c are provided in [17].

3. Models used

Before we proceed to present and discuss the experimental results of the temperature dependence of the critical current density $j_c(T)$ obtained in this work, we will briefly discuss the pinning scaling procedures we used with respect to the $j_c(H)$ dependence [16, 17]. This is important because the results of this scaling will provide additional crucial information for the analysis presented here.

We based the pinning scaling for the $j_c(H)$ dependence on the method proposed by Kramer [21] and significantly developed by Dew-Hughes [22, 23], which predicts the dependence of the pinning force F_p, normalized to its maximum value $F_{p,max}$, on the normalized magnetic field $h = H/H_k$ in the form $f_p = F_p/F_{p,max} = Ah^p(1-h)^q$, where H_k is a certain characteristic critical field (scaling field), A is the proportionality constant, and p and q are scaling exponents characterizing the type of pinning centers. In the Dew-Hughes model, $H_k = H_{c2}$, where H_{c2} is the upper critical field, while in the Kramer model, $H_k = H_K$, where the characteristic field H_K is obtained by extrapolating the critical current density j_c to zero on a graph of $j_c^{0.5}H^{0.25}$ plotted as a function of H [21]. It follows that H_K corresponds to the so-called irreversibility field, H_{irr} (for $H > H_{irr}$, $j_c = 0$ despite $H < H_{c2}$), which differs significantly from H_{c2} for high-temperature superconductors [24]. Due to the method of determination, the scaling field H_K is a lower bound on the irreversibility field obtained by other methods (*e.g.*, from $M(T,H)$ or $R(T,H)$ measurements), and therefore describes properties related to the global critical current flowing through the sample, not to the maximum critical current sustained in some local regions.

In his groundbreaking work, Dew-Hughes defined and analyzed several types of pinning centers, such as atomic vacancies, interstitial atoms, dislocations, foreign phase inclusions, *etc.*, characterizing their geometry as point, linear, surface, or volume [22, 23]. He also considered the nature of the interaction of pinning centers with vortices, distinguishing two basic types: electromagnetically and core-interacting pinning centers. Then, for each of the specified types of pinning, the model determined the effective interaction range, deriving such characteristic quantities as: penetration depth, λ, for electromagnetic pinning with centers of volume geometry, and the distance between adjacent vortices (flux lines), d, coherence length, ξ, and half-size of the pinning center, a, for core pinning with centers of volume, surface, and point geometries, respectively.

For electromagnetically interacting pinning centers, when both the size of the pinning centers, a, and the distance between them, L, are comparable to or larger than λ, in the critical state $a > d$, and therefore in this case, only volume centers should be considered. In turn, for core-interacting pinning centers, when a and/or L are smaller than λ, both volume, surface, and point

centers can be effective. In weak-magnetic fields, when the flux line spacing $d \approx \lambda$, both electromagnetic and core interactions can be important. In high-magnetic fields, due to the decrease in d, core pinning should dominate. Further considering the value of the Ginzburg–Landau parameter, κ_{GL}, it can be assumed that the electromagnetic interaction will have a greater influence on the total pinning force in materials with a low κ_{GL}, where $\lambda > \xi$. In turn, the core interaction should be more effective in materials with a higher κ_{GL}, where $\lambda \gg \xi$. In this case, the larger the κ_{GL}, the stronger the pinning force.

Another distinction between the types of pinning centers relates directly to their conducting (superconducting) properties and distinguishes "normal pinning" and "$\Delta\kappa$ pinning" centers. Normal pinning centers occur when normal (non-superconducting) regions acting as pinning centers for flux lines have dimensions larger than the coherence length ξ. With this assumption, $a > \xi$, regions with weaker superconducting properties than the matrix (lower values of T_c, H_{c2}, j_c) can also act as normal pinning centers. In turn, the $\Delta\kappa$ pinning mechanism applies to situations where normal pinning centers have diameters smaller than ξ. In this case, the proximity effect will induce superconductivity in these centers, but with a change in the Ginzburg–Landau parameter. As mentioned, the result of the discussed pinning force scaling procedure is a specific form of the function $f_p = F_p/F_{p,max} = Ah^p(1-h)^q$, which allows us to determine the type of pinning centers dominant in the studied material [22].

In this paper, we present and analyze the behavior of critical current density as a function of temperature in Y123 single crystals to shed more light on the nature of the enhanced vortex pinning force (and therefore also j_c) due to Mo substitution. We analyze the results with respect to the normal or superconducting properties of the pinning centers, which influence the mechanism of interaction between these centers and the vortices. The general approach allows us to distinguish two basic types of this mechanism: the δl pinning, which results from spatial variations in the electron mean free path, and the δT_c pinning, which is induced by fluctuations in the superconducting transition temperature [18, 25]. In other words, the δl pinning is provided by non-superconducting regions, while the δT_c pinning is provided by regions with impaired superconductivity (regions with reduced T_c). The δl pinning is most often responsible for the j_c in weak-magnetic fields (easy penetration of normal regions), while the δT_c pinning usually involves high-magnetic fields to suppress superconductivity at superconducting pinning centers. In Y123, and more generally, in copper–oxide superconductors, oxygen vacancies can play a dominant role in controlling the pinning strength. Interestingly, they can act as both the δl and δT_c pinning centers [18].

4. Results and discussion

Example results of the dependence of the critical current density on the magnetic field $j_c(H)$ are presented in Fig. 1 for two Mo-substituted single crystals annealed under low (YMo2–LPA) and high (YMo2–LPA–HPA) oxygen pressure. For the YMo2–LPA–HPA single crystal, *i.e.*, the YMo2-LPA single crystal annealed again under high oxygen pressure (HPA), a clear increase in j_c with increasing H is observed (the so-called peak effect), which

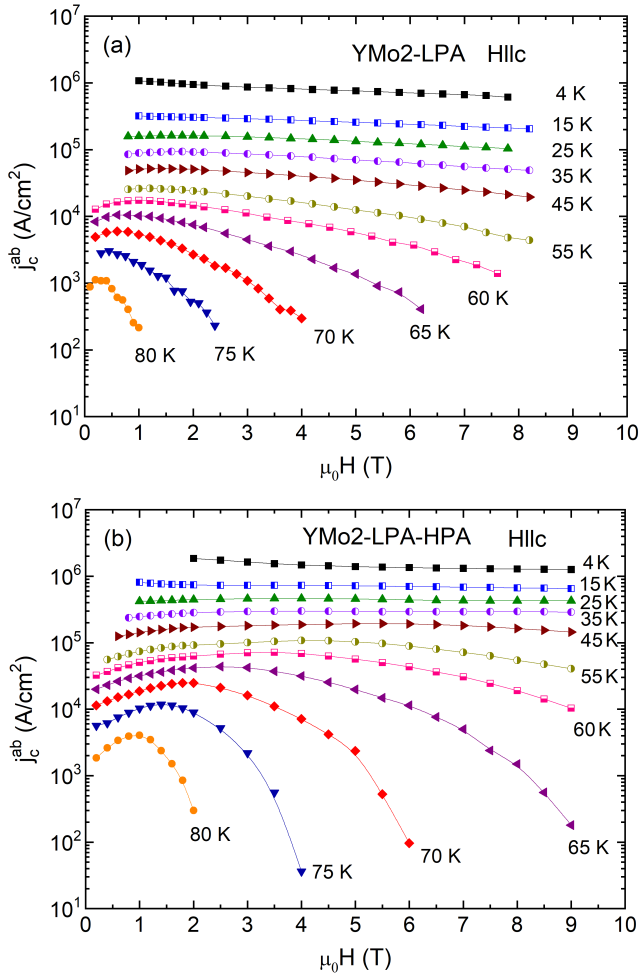

Fig. 1. Critical current density in the *ab*-plane at different temperatures as a function of magnetic field for two Mo-substituted single crystals annealed (a) under low oxygen pressure (YMo2–LPA) and (b) under high oxygen pressure (YMo2–LPA–HPA). The magnetic field was oriented parallel to the *c*-axis ($H||c$), which corresponds to j_c in the *ab*-plane.

appears at temperatures above 35 K and shifts toward lower H at higher temperatures. The appearance of the peak effect indicates an increase in the pinning force for the Mo-substituted crystals, as clearly demonstrated by the analysis of the results conducted within the framework of scaling theory [17]. Based on similar $j_c(H)$ plots, the $j_c(T)$ and then $j_c(t)$ dependencies were obtained, where $t = T/T_c$, for several magnetic fields for all four single crystals studied.

The temperature dependence of the reduced critical current density $j_c(t)/j_c(0)$ for the single crystal without Mo substitution, annealed under low oxygen pressure, Y123–LPA, is shown in Fig. 2. The values of $j_c(0)$ for different H were obtained by extrapolating $j_c(T)$ to $T = 0$. Since this procedure involves some extrapolation freedom, the value of j_c at temperature $T = 4.2$ K, $j_c(4\,\mathrm{K})$, was also determined and $j_c(t)/j_c(4\,\mathrm{K})$ was calculated, as shown in the inset to Fig. 2. As can be seen from the comparison, the results do not differ qualitatively and only show a slight increase in the value of $j_c(t)/j_c(4\,\mathrm{K})$ with respect to $j_c(t)/j_c(0)$. In the following figures, we present more practical and, importantly, free from extrapolative arbitrariness $j_c(t)/j_c(4\,\mathrm{K})$ relationships, which we analyze.

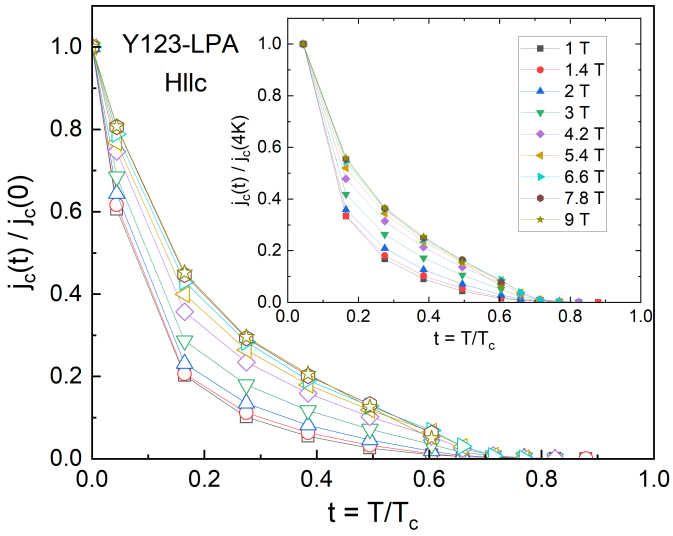

Fig. 2. Temperature dependencies of the reduced critical current density $j_c(t)/j_c(0)$ at different magnetic fields, for Y123–LPA, *i.e.* the single crystal without substituted Mo, annealed under low oxygen pressure. The inset shows $j_c(t)/j_c(4\,\mathrm{K})$, where $j_c(4\,\mathrm{K})$ denotes the value of j_c at $T = 4.2$ K. The magnetic field was oriented parallel to the c-axis ($H||c$).

As mentioned, the pinning force and thus the magnitude of critical currents in superconductors are governed by two dominant mechanisms: the δT_c pinning, which is related to the spatial fluctuation of T_c, and the δl pinning, which denotes fluctuations in the mean free path of charge carriers. In the case of δT_c pinning, the normalized critical current density has the form $j_c(t)/j_c(0) = (1-t^2)^{7/6}(1+t^2)^{5/6}$, while in the case of δl pinning, $j_c(t)/j_c(0) = (1-t^2)^{5/2}(1+t^2)^{-1/2}$, where, as before, $t = T/T_c$ [18, 25]. Figure 3 shows once again the experimental results of $j_c(t)/j_c(4\,\mathrm{K})$ for the Y123–LPA single crystal in comparison with the theoretical relations. The $j_c(t)$ dependencies were determined for magnetic fields ranging from 1 to 9 T oriented parallel to the c-axis ($H||c$). The results do not scale well with any of the expected theoretical dependencies, which is interesting given the observation of a clear δl pinning scaling in Y123 superconducting films [25]. We can only discuss the general nature of the obtained $j_c(t)$ dependencies, which appears to be consistent with the δl pinning. As can be easily seen, at intermediate temperatures ($t = 0.2$–0.6), the $j_c(t)$ values increase approximately linearly with increasing $\mu_0 H$ up to 4 T, after which they saturate. Because a similar trend occurs for all single crystals studied here (as long as $j_c(t)$ clearly depends on H), for clarity, we will present further results only for a few selected magnetic fields $\mu_0 H = 1$, 3, 5, and 7, 8, or 9 T, depending on the availability of experimental data.

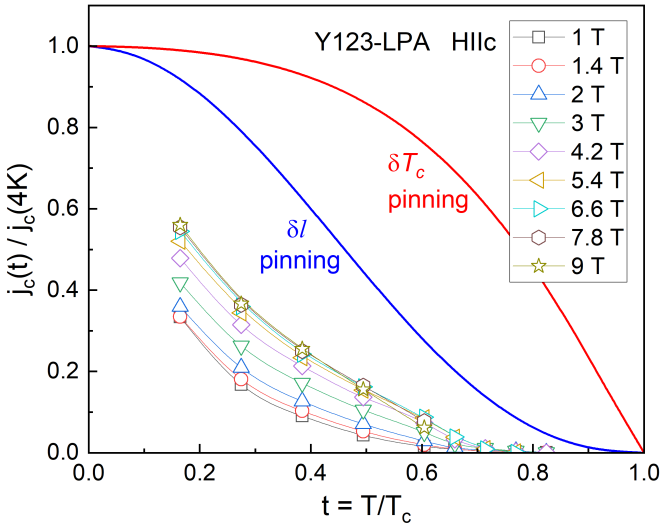

Fig. 3. Temperature dependences of the critical current density $j_c(t)/j_c(4\,\mathrm{K})$ at different magnetic fields, for the Y123–LPA single crystal compared with theoretical predictions for the δl and δT_c pinning. The magnetic field was oriented parallel to the c-axis ($H||c$).

The increase in $j_c(t)$ observed for the Y123–LPA single crystal with increasing H obviously indicates the occurrence of a strong, so-called second magnetization peak (fishtail effect) for the $M(H)$ dependence, as shown in Ref. [17]. For this single crystal, there is no scaling of the pinning force $f_p = F_p/F_{p,max}$, *i.e.*, meaning that the $f_p(h)$ curves are not similar for different temperatures [17]. Therefore, in this material, there is no dominant type of pinning center, and the efficiency of different types of centers changes with the change in the coherence length $\xi(T)$.

The $j_c(t)$ dependence for the single crystal annealed in oxygen at high pressure, Y123–HPA, is shown in Fig. 4. The nature of the dependence is like that for Y123–LPA, where the δl-type pinning mechanism dominates, but the $j_c(t)$ values are clearly higher at lower temperatures. Moreover, this material exhibits some scaling of the pinning force, as shown in the inset to this figure. For low H, the $f_p(h)$ dependence roughly follows the $h(1-h)$ plot, suggesting core-interacting volume-geometry $\Delta\kappa$ (core-volume-$\Delta\kappa$) pinning. In turn, at higher H, $f_p(h) = A \cdot h(1-h)^2$, which may indicate the emergence of dominant core-point-normal pinning centers [22]. These pinning centers in Y123–HPA, formed by annealing under high oxygen pressure, may be

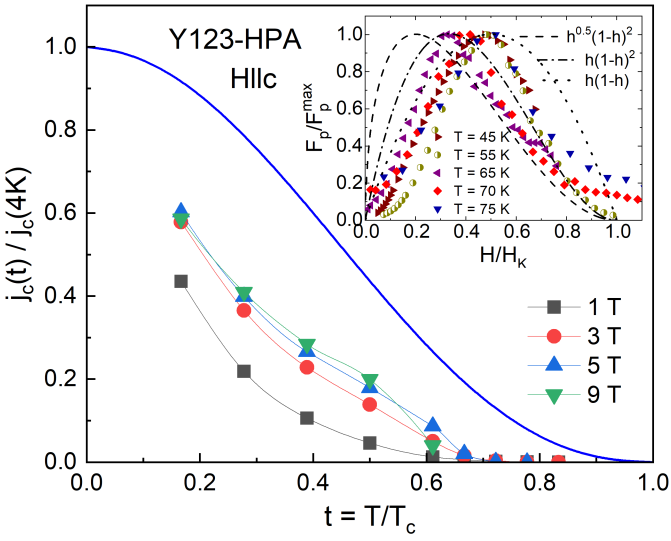

Fig. 4. Reduced critical current density $j_c(t)/j_c(4\,\mathrm{K})$ at different magnetic fields as a function of reduced temperature for Y123–HPA, *i.e.*, the single crystal without substituted Mo, annealed under high oxygen pressure. The solid blue line denotes the theoretical dependence for the δl pinning. The magnetic field was oriented parallel to the c-axis ($H||c$). The inset shows the scaling of the pinning force as described in the text (figure taken from Ref. [16]).

oxygen clusters and interstitial oxygen, in weak- and high-magnetic fields, respectively. Overall, the scaling effect is weakly visible, so the above conclusions are rather speculative.

The situation is quite different for Mo-substituted single crystals. Figure 5 shows the $j_c(t)$ dependence for the single crystal annealed in oxygen at low pressure, YMo2–LPA. Although the general pinning mechanism is the same as for the single crystal without Mo substitution, the lack of a clear dependence of the critical current density on the magnetic field is striking, indicating the absence of a $j_c(H)$ peak in this material in the range of H we studied. In turn, as shown in the inset to Fig. 5, YMo2–LPA exhibits quite good scaling, $f_p = A \cdot h^p(1-h)^q$, for $p = 0.5$ and $q = 2$, indicating that core-interacting normal (non-superconducting) pinning centers with a surface shape (core-surface-normal) dominate in this material, at least for higher H values, above the $f_p(h)$ maximum.

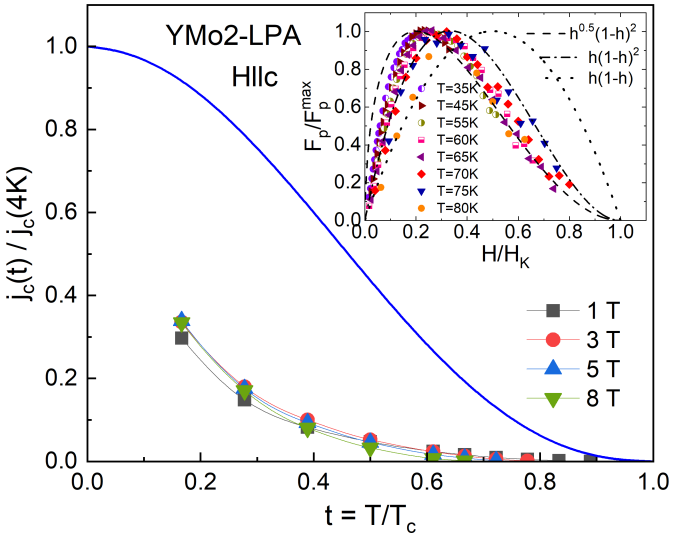

Fig. 5. Reduced critical current density $j_c(t)/j_c(4K)$ at different magnetic fields as a function of reduced temperature for YMo2–LPA, *i.e.*, the single crystal with Mo substituted for Cu in the CuO chain, annealed under low oxygen pressure. The solid blue line denotes the theoretical dependence for the δl pinning. The magnetic field was oriented parallel to the c-axis ($H||c$). The inset shows the scaling of the pinning force as described in the text (figure taken from Ref. [16]).

The dependence of $j_c(t)$ waveforms on the magnetic field returns for the single crystal with substituted Mo annealed in high oxygen, YMo2–LPA–HPA, with maintaining the δl-type pinning mechanism, as shown in Fig. 6. For this material, we observe almost a perfect scaling of the pinning

force, the nature of which, interestingly, changes with the magnitude of the magnetic field (see inset to Fig. 6). For low H, the agreement between the experimental results and the model occurs for $p = 1$ and $q = 1$, which indicates core-volume-$\Delta\kappa$ pinning, while for high H, this agreement occurs for $p = 1$ and $q = 2$, which indicates core-point-normal pinning. As can be seen from the figure, the scaling occurs over a wide temperature range, from the lowest to 80 K (a slight deviation appears above 70 K). However, scaling below 45 K is not possible due to the inability to determine the critical field H_{K}, whose values are not available at these temperatures in fields up to 14 T [17].

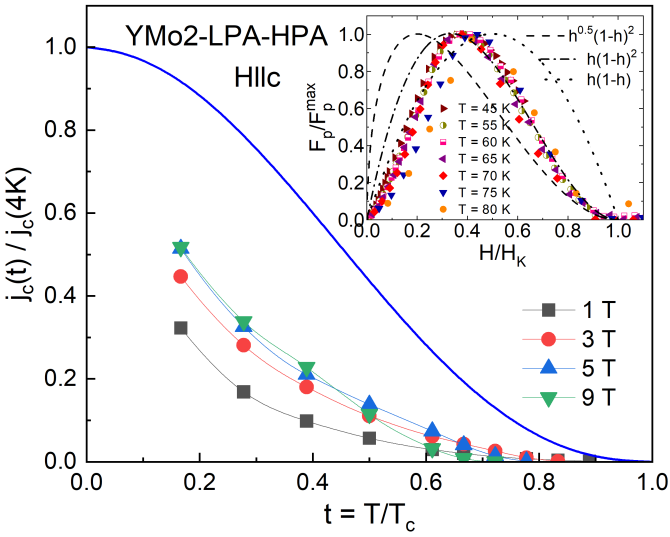

Fig. 6. Reduced critical current density $j_{\mathrm{c}}(t)/j_{\mathrm{c}}(4\,\mathrm{K})$ at different magnetic fields as a function of reduced temperature for YMo2–LPA–HPA, *i.e.*, the single crystal with Mo substituted for Cu in the CuO chain, annealed under low and then high oxygen pressure. The solid blue line denotes the theoretical dependence for the δl pinning. The magnetic field was oriented parallel to the c-axis ($H||c$). The inset shows the scaling of the pinning force as described in the text (figure taken from Ref. [16]).

As shown in our previous work on powder materials, Mo introduced into Y123 substitutes pairwise for Cu in CuO chains, forming Mo_2O_{11} octahedra dimers along and/or across these chains [14, 15]. These dimers constitute effective pinning centers to an extent dependent on the amount of oxygen supplied. In the case of the YMo2–LPA single crystal, we identify these centers as incompletely oxidized Mo–O clusters, because YMo2–LPA was annealed in oxygen at most likely insufficiently high pressure. In this case,

these clusters are rather small, diffuse defects that can only act as moderately effective pinning centers. In turn, the high-pressure annealing of YMo2–LPA forces the full oxygenation and formation of the Mo_2O_{11} octahedra dimers, making them well-defined (well-formed) defects in the YMo2–LPA–HPA single crystal. Additionally, fully oxidized dimers can aggregate to form larger-volume defects, *e.g.*, four connected MoO_6 octahedra replacing a square of four Cu ions, and thus can act as true volume pinning centers [14, 15]. Annealing in oxygen under high pressure (HPA) likely also results in the appearance of interstitial oxygen, which can additionally cluster. In summary, the defects produced, both well-formed dimers and interstitial oxygen, act as effective volume and point pinning centers, respectively.

For the YMo2–LPA–HPA single crystal, which for the $H||c$ configuration showed full scaling of the pinning force over a wide temperature range (see the inset to Fig. 6), we further analyzed $j_c(t)$ for H parallel to the ab-plane ($H||ab$), as shown in Fig. 7. The presented results show a much weaker dependence of $j_c(t)$ on the magnetic field than for $H||c$, which indicates a change in the type of dominant pinning centers for this configuration. Also, the analysis of the dependence of the pinning force on H (see the inset to Fig. 7) indicates a new type of such centers, for which the $f_p(h)$ scaling

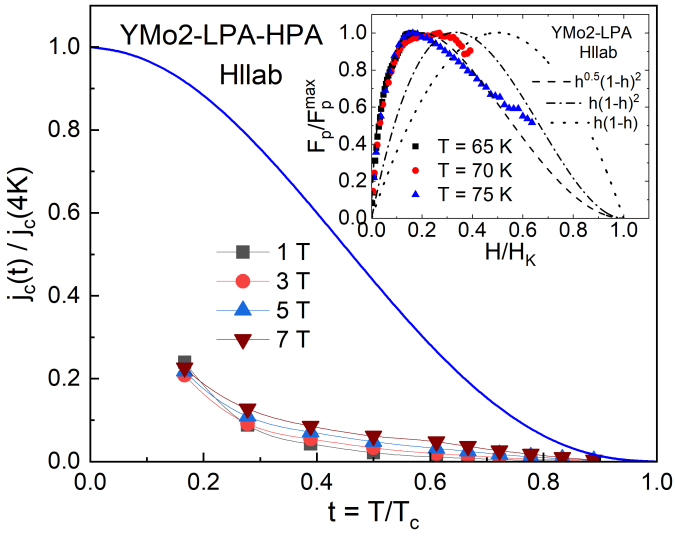

Fig. 7. Reduced critical current density $j_c(t)/j_c(4\,\mathrm{K})$ at different magnetic fields as a function of reduced temperature for the YMo2–LPA–HPA single crystal, the same as in Fig. 6. For these measurements, the magnetic field was oriented parallel to the ab-plane ($H||ab$). The inset shows the scaling of the pinning force as described in the text (figure taken from Ref. [17]).

was obtained only in a narrow temperature range, 65–75 K, and only for weak magnetic fields ($h < 0.2$). As can be seen from the figure, this new type of pinning centers is core-surface-normal, which fits perfectly with the common knowledge on this subject. It is believed that for the $H||ab$ configuration, the most effective pinning centers are the weakly conducting (non-superconducting) quasi-two-dimensional regions between the CuO_2 planes, where quasi-normal vortex cores are located.

5. Conclusions

We have analyzed the types of pinning centers present in Y123 and Mo-substituted Y123 single crystals annealed at low and high oxygen pressure. As can be seen from figures 4–7, the δl-type pinning mechanism dominates in all studied single crystals. This is also confirmed by the results showing the scaling of the pinning force (insets to figures 4–7), where the maximum in $f_p(h) = F_p(h)/F_{p,max}$ occurs at $h < 0.5$, while in the case of the δT_c-type pinning mechanism, it is expected to occur at $h > 0.5$. Our experimental results differ quantitatively from those previously reported for Y123 thin films [25] and for Dy123 single crystals [26], where the δl-type pinning was also observed. In turn, our results differ qualitatively for single crystals of Y123 doped with Pr [27] and for textured bulk materials of Y123 doped with Zn [28], where the δT_c-type pinning occurred. This is most likely because in those materials, the dominant types of pinning centers were most likely oxygen vacancy clusters [26], Pr123 phase inclusions [27], and the induced magnetic moments caused by the substitution of Zn for Cu in the CuO_2 planes [28]. In our single crystals, the introduced centers are Mo_2O_{11} octahedra dimers and interstitial oxygen atoms and/or oxygen clusters, which act with different efficiency or by a completely different mechanism.

For all our single crystals, the identified type of vortex-pinning center interaction is of a "core" nature, which is justified by the fact that the sizes of the introduced pinning centers (Mo_2O_{11} octahedra dimers and interstitial oxygen atoms and clusters) are smaller in all directions than the Y123 penetration depth. Further, depending on the amount of introduced oxygen, we define the type of pinning centers as: core-volume-$\Delta\kappa$ in weak H and core-point-normal in high H, both for Y123–HPA (suboptimal scaling) and YMo2–LPA–HPA (perfect scaling), the single crystals annealed in oxygen at high pressure. The observed types of pinning centers: core-surface-normal for YMo2–LPA and core-volume-$\Delta\kappa$ for YMo2–LPA–HPA are explained by the occurrence of insufficiently oxygenated Mo–O clusters, and fully oxygenated Mo_2O_{11} octahedra dimers, respectively. Moreover, as a result of annealing under high oxygen pressure (HPA), Mo_2O_{11} dimers can form larger volume defects, *e.g.*, four connected MoO_6 octahedra replacing

a square of four Cu ions, and thus can act as true bulk pinning centers [14, 15]. In turn, the core-point-normal pinning centers observed for HPA single crystals in high-magnetic fields appear to be caused by the appearance of interstitial oxygen, *i.e.*, point-like defects, in the structure.

It should also be noted that although the relative values of $j_c(t)/j_c(4K)$ do not vary regularly with the expected number of pinning centers introduced in different single crystals, the absolute values of $j_c(t)$ generally increase as we move from Y123–LPA, through Y123–HPA, to YMo2–LPA, and then to YMo2–LPA–HPA, as shown in our previous works [16, 17]. Our studies provide insight into what general type and more specific type of pinning centers should be effective in Y123-type materials under various magnetic fields and temperatures.

REFERENCES

[1] T. Oka, K. Yokoyama, «Magnetic Behavior of High-Temperature Superconducting Bulk Magnets and their Industrial Applications», *IEEJ Trans.* **21**, 4 (2026), and references therein.

[2] A. Molodyk, D.C. Larbalestier, «The prospects of high-temperature superconductors», *Science* **380**, 1220 (2023), and references therein.

[3] M. Calvi *et al.*, «GdBCO bulk superconducting helical undulator for x-ray free-electron lasers», *Phys. Rev. Res.* **5**, L032020 (2023).

[4] J.L. MacManus-Driscoll, S.C. Wimbush, «Processing and application of high-temperature superconducting coated conductors», *Nature Rev. Mat.* **6**, 587 (2021).

[5] W.I.F. David *et al.*, «Structure and crystal chemistry of the high-T_c superconductor $YBa_2Cu_3O_{7-x}$», *Nature* **327**, 310 (1987).

[6] P.N. Mikheenko, S.X. Dou, S.J. Lewandowski, I.S. Abaliosheva, «Quasi-2D behaviour of HTSCs: the consequence of the small effective thickness of superconducting layers», *Supercond. Sci. Technol.* **9**, 942 (1996).

[7] V.I. Nizhankovskiy, K. Rogacki, «BKT transition observed in magnetic and electric properties of $YBa_2Cu_3O_{7-\delta}$ single crystals», *Phys. Rev. B* **100**, 104510 (2019).

[8] D. Larbalestier, A. Gurevich, D.M. Feldmann, A. Polyanskii, «High-T_c superconducting materials for electric power applications», *Nature* **414**, 368 (2001).

[9] X. Obradors, T. Puig, «Coated conductors for power applications: materials challenges», *Supercond. Sci. Technol.* **27**, 044003 (2014).

[10] C. Senatore *et al.*, «Progresses and challenges in the development of high-field solenoidal magnets based on RE123 coated conductors», *Supercond. Sci. Technol.* **27**, 103001 (2014).

[11] A.J. Creely *et al.*, «SPARC as a platform to advance tokamak science», *Phys. Plasmas* **30**, 090601 (2023).

[12] C. Gao *et al.*, «40 Tesla miniature magnets», *Sci. Adv.* **12**, 5826 (2026).

[13] D.G. Kuberkar *et al.*, «Flux pinning and critical currents by Mo-substitution in $YBa_2Cu_3O_{7-\delta}$», *Appl. Supercond.* **3**, 357 (1995).

[14] K. Rogacki, B. Dabrowski, O. Chmaissem, J.D. Jorgensen, «Increase of the superconducting T_c, irreversibility fields, and critical currents in tetragonal $YBaSrCu_{3-x}Mo_xO_{7+d}$», *Phys. Rev. B* **63**, 054501 (2000).

[15] K. Rogacki, B. Dabrowski, O. Chmaissem, «Increase of critical currents and peak effect in Mo-substituted $YBa_2Cu_3O_7$», *Phys. Rev. B* **73**, 224518 (2006).

[16] A. Los, B. Dabrowski, K. Rogacki, «Increase of $YBa_2Cu_3O_7$ critical currents by Mo substitution and high-pressure oxygen annealing», *Current Appl. Phys.* **27**, 1 (2021).

[17] K. Rogacki, A. Los, B. Dabrowski, «Raising critical currents in YBaCuO-type high-temperature superconductors by Mo substitution», *Low Temp. Phys.* **49**, 364 (2023).

[18] G. Blatter *et al.*, «Vortices in high-temperature superconductors», *Rev. Mod. Phys.* **66**, 1125 (1994).

[19] M.R. Koblischka, M. Murakami, «Pinning mechanisms in bulk high-T_c superconductors», *Supercond. Sci. Technol.* **13**, 738 (2000).

[20] C.P. Bean, «Magnetization of Hard Superconductors», *Phys. Rev. Lett.* **8**, 250 (1962); «Magnetization of High-Field Superconductors», *Rev. Mod. Phys.* **36**, 31 (1964).

[21] E.J. Kramer, «Scaling laws for flux pinning in hard superconductors», *J. Appl. Phys.* **44**, 1360 (1973).

[22] D. Dew-Hughes, «Flux pinning mechanisms in type II superconductors», *Philos. Mag.* **30**, 293 (1974).

[23] D. Dew-Hughes, «The role of grain boundaries in determining J_c in high-field high-current superconductors», *Philos. Mag.* **55**, 459 (1987).

[24] Y. Yeshurun, A.P. Malozemoff, A. Shaulov, «Magnetic relaxation in high-temperature superconductors», *Rev. Mod. Phys.* **68**, 911 (1996).

[25] R. Griessen *et al.*, «Evidence for mean free path fluctuation induced pinning in $YBa_2Cu_3O_7$ and $YBa_2Cu_4O_8$ films», *Phys. Rev. Lett.* **72**, 1910 (1994).

[26] A.J.J. van Dalen *et al.*, «Dynamic contribution to the fishtail effect in a twin-free $DyBa_2Cu_3O_{7-\delta}$ single crystal», *Physica C* **250**, 265 (1995).

[27] H.H. Wen *et al.*, «Evidence for flux pinning induced by spatial fluctuation of transition temperatures in single domain $(Y_{(1-x)}Pr_x)Ba_2Cu_3O_{7-\delta}$», *Physica C* **251**, 371 (1995).

[28] G. Krabbes *et al.*, «Zn doping of $YBa_2Cu_3O_7$ in melt textured materials: peak effect and high trapped fields», *Physica C* **330**, 181 (2000).